Effects of mild hallux valgus on forefoot biomechanics during walking: a finite element analysis

Yan Zhang, Jan Awrejcewicz

Abstract: Hallux valgus (HV) is a common foot deformity characterized by progressive lateral deviation of the hallux with medial deviation of the first metatarsal. In this study, foot models of a normal subject and a mild HV hallux valgus patient were developed to evaluate the effects of mild HV on forefoot biomechanics during walking. Three-dimensional finite element model of a normal foot and a mild HV foot were constructed. Finite element analysis was conducted in ANSYS Workbench 17.0. The biomechanical performances were compared at three gait instants, first-peak, mid-stance, and second-peak. The equivalent stress on five metatarsals increased while the resultant joint force and the contact pressure of the first metatarsophalangeal joint (MTP) decreased in mild HV foot in comparison of normal foot. At push-off instant, the normal foot presented a concentrated pressure under the more distal portion of the metatarsal and the hallux, while the HV foot exhibited a more evenly distributed pattern with concentrated pressure under more proximal location of the metatarsal and the hallux. The predicted alternations in joint loading and plantar pressure distribution pattern of the HV foot indicated that HV feet may have deficient capability of body weight transfer at the first MTP during walking.

1. Introduction

Hallux valgus (HV) is one of the most common foot deformities with the high prevalence of 23% in adult and 35.7% in elderly population [1]. It is characterized by the progressive subluxation and valgus angulation of the first metatarsophalangeal joint in combination with pronation of the proximal phalanx. Increasing HV severity often induces problems of foot pain [2], metatarsalgia [3], and balance defects [4]. More and more elderly people complain instability and risk of falling, particularly when walking on irregular terrain [2]. In addition, the deformity of foot structure is very likely to impair these biomechanical functions. The fact is that there is no scientific data so far to evidence this speculation and to completely explain the painful phenomenon in HV feet. Research on biomechanical behaviour of the deformed foot should be carried out to provide fundamental and systematic knowledge for the development of podiatrics and orthopaedics.

The metatarsal bones act as a unit in the forefoot to provide a broad plantar surface for load bearing. Various in vivo studies that evaluated risks at metatarsals regarding to HV have focused on potential overloading and altered weigh bearing pattern by plantar pressure measurements. Increased forefoot

plantar pressure has been evidenced in HV feet; however, debate remains in the forefoot regions where the alternation occurs. Bryant et al. [5] suggested that peak pressure of HV foot increased significantly under the first, second and third metatarsal heads compared with normal foot. Plank [6] also observed a medial shift of peak pressure in HV patients. On the contrary, there is research reporting increased load on lateral metatarsals [7]. Koller et al. [8] assessed the plantar pressure of HV feet of different grades and concluded a positive correlation between HV grade and peak pressure of the fifth metatarsal head.

FE model is capable of simulating complicated boundary and loading conditions and predicting the internal stress/strain in the foot complex. As the deformities of the complex foot structures increase the challenge in the modeling process, few studies concern FE models of deformed foot. It is of high significance to take insight into the biomechanical behavior of HV foot which is an increasingly prevalent foot deformity, particularly in the elderly population. Using FE method to develop numerical models of the deformed feet is an important step in the investigation of foot kinematical and mechanical manifestation during locomotion. This study aimed to establish an enhanced approach to predicting injury risk and evaluating biomechanical function efficiency of HV deformed foot. Knowledge of this project could improve the understanding of the underlying mechanisms of structural mechanical problems and abnormal gait pattern of mild HV feet.

2. Method

The three-dimensional models of the normal foot and the HV foot were reconstructed from computer tomography (CT) images of a 26-year old female (height: 165cm; weight: 51kg) and a 29-year old female (height: 163cm; weight: 54kg) respectively. Both participants had no other musculoskeletal pathology, pain, or lower limb injury or surgery within the past 12 months.

The coronal CT images were obtained with a space interval of 2 mm without weight-bearing. The images were segmented using MIMICS 16.0 (Materialise, Leuven, Belgium) to obtain the boundaries of the skeleton and the soft tissue. The geometry of the skeletal components and the soft tissue were processed using Geomagic Studio 2013 (Geomagic, Inc., Research Triangle Park, NC, USA) to smooth the uneven surface caused by the stacking of the medical images. Each surface component was then imported into Solidworks 2016 (SolidWorks Corporation, Massachusetts, USA) individually to form solid parts. To ensure the alignment of the exterior surfaces of the assembled model, cartilages were created using Boolean operations by subtracting one bony object with the adjacent one to connect the two bones and fill the cartilaginous spaces. The encapsulated soft tissue was subtracted from the whole foot volume by the bony and cartilaginous structures. The whole foot model consisted of 28 foot bony segments, including tibia, fibula, talus, calcaneus, cuboid, navicular, three cuneiforms, five metatarsals and 14 phalanges. Link elements that have only tension function capability were used to simulate

ligaments bearing the tension load. A total number of 76 ligaments and five plantar fascia were included and defined by connecting corresponding anatomical locations on the bones by reference to an anatomy book [9]. HyperMesh 13.0 (Altair Engineering Inc., Hyperworks, America) was used for mesh generation. Each bony and cartilaginous component and the soft tissue were partitioned based on the anatomical structure and were meshed as Hexahedral dominant elements. The FE package ANSYS Workbench 17.0 (ANSYS, Inc., Canonsburg, USA) was used for subsequent analysis. Automated surface-to-surface contact algorithm in ANSYS Workbench was used to simulate the interaction of the surfaces of the cartilaginous and bony structures. All the bones and cartilages were bonded to the encapsulated soft tissue.

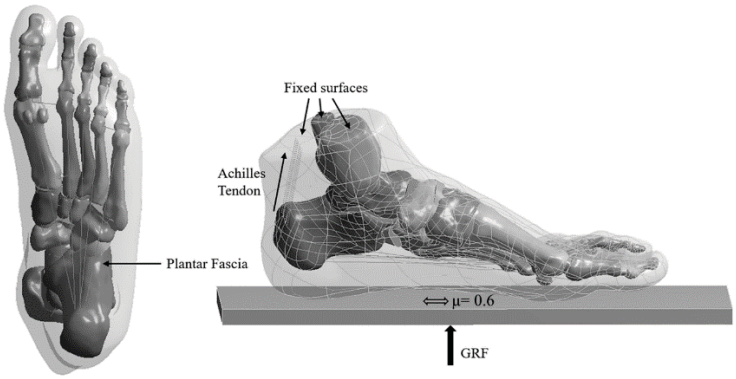

Figure 1. The three-dimensional finite element model and the application of boundary and loading conditions.

All the materials except for the soft tissue were considered isotropic and linearly elastic with material properties obtained from previous literature [10, 11]. The two material constants of Young's modulus E and Poisson's ratio ν were given to describe the elasticity. The encapsulated soft tissue was set as nonlinear hyperelastic material which was defined as Moonley-Rivlin model. The element types and material properties used are listed in Table 1 and Table 2.

Table 1 Material properties and mesh element types for the foot model components.

Component	Element Type	Young's Modulus (MPa)	Poisson's Ratio	Cross-section Area (mm^2)
Bone	Hexahedral solid	7300	0.3	-
Cartilage	Hexahedral solid	1	0.4	-

Ligaments	Tension-only spar	260	0.4	18.4
Plantar Fascia	Tension-only spar	350	0.4	58.6
Plate	Hexahedral solid	17000	0.4	-

Table 2 The element type and coefficients of the hyperelastic material used for the encapsulated soft tissue.

Element Type	C10	C01	C20	C11	C02	D1	D2
Hexahedral solid	0.08556	-0.05841	0.03900	-0.02319	0.00851	3.65273	0.00000

Stance phase was simulated by applying GRF and tibial inclination. The input data were originated from the gait experiment of the same participant. Three instants were extracted in the following percentage stance phase: 0% (heel-strike), 27% (GRF first peak), and 75% (GRF second peak). The percent-age maximum voluntary contraction of muscles corresponding to these instants were adopted [12] and multiplied by their maxi-mum force [13] for the calculation of muscle forces at the selected instants. The superior surfaces of the encapsulated soft tissue, distal tibia and distal fibula were fixed. The foot-ground interaction was simulated as a foot-plate system (Fig. 1). The plate was assigned with an elastic property to simulate the concrete ground support. The interaction between the foot plantar surface and the superior surface of the plate was simulated as contact with friction. The coefficient of friction was set to 0.6 [14]. Five equivalent force vectors representing the Achilles tendon force were applied over the area of the posterior extreme of the calcaneus.

The numerical model was validated by comparing plantar pressure obtained from computational simulation in FE software and experimental measurement by a Novel emed pressure platform (Novel, Munich, Germany) in standing position. For FE simulation of balanced standing, vertical GRF of half-body weight was applied at the inferior surface of the plate; and the force of Achilles tendon force was estimated as 50% of the force acting on the foot [11]. The validated models were then used for FE analysis on forefoot biomechanics.

3. Results

Three-dimensional FE models were validated by plantar pressure measurement. This method was commonly used in the validation of finite element foot model [11]. Fig. 2 shows the comparison of

predicted plantar pressure of the normal foot with experimental results. The predicted peak pressure and the pressure distribution pattern were generally agreeable with those from measurement. The peak pressure from numerical models and experimental measurement was 0.141MPa and 0.135MPa respectively, and both located at the heel region.

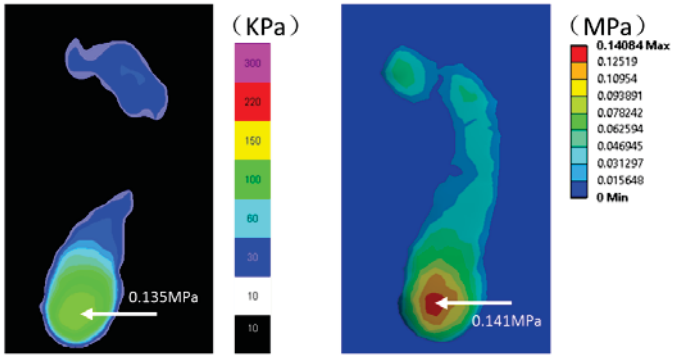

Figure 2. Comparison of the plantar pressure between experimental measurement and computational prediction in balanced standing position.

Previous experimental results advocated medial or lateral shift of forefoot plantar pressure due to HV deformity. As to von-Mises stress at the five metatarsals, stress distribution remains unchanged. The metatarsals of the HV foot sustained higher von-Mises stress (Fig. 3). It is possible to speculate that the increased metatarsal stress may cause metatarsalgia while weight bearing. The most obvious increasing of von-Mises stress at the first metatarsal indicates that this metatarsal is more susceptible to injury, such as stress fractures [15] and pain. The first metatarsal should be expected to avoid sustaining high stress during weight bearing in view of the first ray deformity. This is very likely to be associated with medial arch collapse which is often thought to supervene with hallux valgus [16].

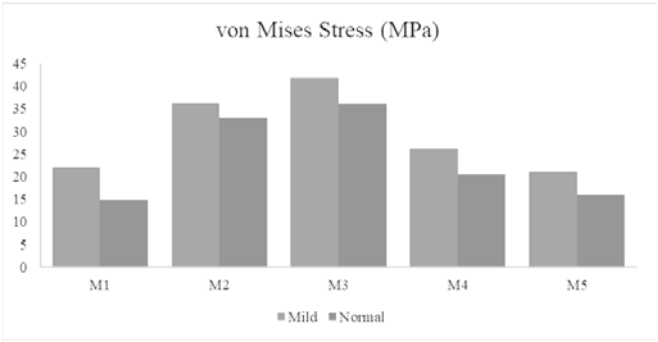

Figure 3. Comparison of von-Mises stress at five metatarsals between normal and hallux valgus foot.

Contact pressure of MTP joints was lower in HV foot (Fig. 4). Also, the resultant joint force of the first MTP showed lower magnitude compared to that of normal foot (Fig. 5). The decreased joint loading may imply the impairment of load bearing and transfer function of the first MTP joint in gait. In agreement with this speculation, Zhang et al. [17] found weakened windlass mechanism in HV foot during initial push-off. In contrast to the location of central bottom on the cartilage for the normal foot, it shifts to medial bottom for the HV foot, which may aggravate the symptom of "painful bunion" which is one of the most common complaints among HV patients [18]. Moreover, the component joint force in the medial-lateral direction presented to be opposite between HV and normal foot. The HV foot shows lateral reaction force at the first MTP joint during balanced standing, suggesting that loading of body weight alone could predispose the patient to the risk of developing HV deformity.

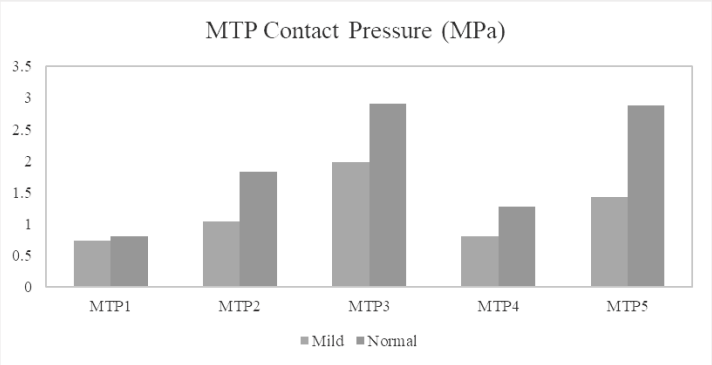

Figure 4. Comparison of contact pressure at the first metatarsophalangeal joint between normal and hallux valgus foot.

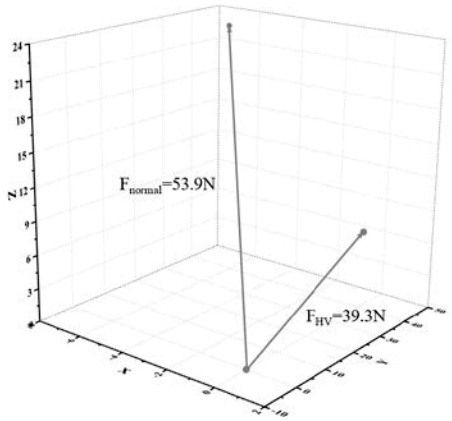

Figure 5. Comparison of joint force at the first metatarsophalangeal joint between normal and hallux valgus foot.

The ratio of peak plantar pressure between the hallux and the first MTP indicates different plantar pressure pattern between normal foot and mild HV foot. The ratio is 1.8 and 2.1 for the normal foot and HV foot respectively, which suggests that the normal foot exhibited a concentrated pressure closer to distal portion of the metatarsal, by contrast, the HV foot presented a more evenly distributed pattern with concentrated pressure at a more proximal location. This reinforces the notion of impaired windlass function in gait due to hallux valgus.

The FE models in this study were based on some simplifications and assumptions. First, cortical and cancellous bone was considered as a single homogeneous component with linear elastic properties. Second, this study created a representative single-subject model of a mild hallux valgus foot. The foot structure, such as arch height and toe deformity, may vary among hallux valgus feet; therefore, the presented data should be considered as a first rough approximation. Third, although hallux valgus is prominently characterized by skeletal deformity, it is also thought to be associated with ligamentous laxity and hypermobility of the first metatarsophalangeal joint [19]. For further study, the material properties of soft tissues should be assumed based on patient-specific model.

4. Conclusions

The first initiative of this project is to develop deformed FE models of a mild HV foot and a HV foot. Furthermore, since hexahedral elements were indicated to provide a more accurate and efficient foundation in structural analysis, all solid parts in this research will be initially meshed into hexahedral elements rather than tetrahedral elements that are commonly relied on in mesh generation of human foot models so far. Moreover, instead of simulating the main bone interactions as contacting deformable bodies, this research will initially create cartilaginous volumes using Boolean operations by subtracting the adjacent bones to fill the spaces between the bones.

Generally, the equivalent stress on five metatarsals increased while the resultant joint force of the first MTP decreased in HV foot in comparison of normal foot. At push-off instant, the normal foot presented a concentrated pressure under the more distal portion of the metatarsal and the hallux, while the HV foot exhibited a more evenly distributed pattern with concentrated pressure under more proximal location of the metatarsal and the hallux. The predicted alternations in joint loading and plantar pressure distribution pattern of the HV foot indicated that HV feet may have deficient capability of body weight transfer at the first MTP during walking.

References

[1] S. Nix, M. Smith, B. Vicenzino, Prevalence of hallux valgus in the general population: a systematicreview and meta-analysis. *J Foot Ankle Res* 3, 1 (2010), 1-9.

[2] Menz, H.B., Lord, S.R. Gait instability in older people with hallux valgus. *Foot Ankle Int* 26, 6 (2005), 483-489.

[3] Waldecker, U. Metatarsalgia in hallux valgus deformity: a pedographic analysis. *J Foot Ankle Surg* 41, 5 (2002), 300-308.

[4] Menz, H.B., and Lord, S.R. The contribution of foot problems to mobility impairment and falls in community‐dwelling older people, *J Am Geriatr Soc* 49, 12 (2001), 1651-1656.

[5] Bryant, A.P., Tinley, P., Singer, K. Plantar pressure distribution in normal, hallux valgus and hallux limitus feet. *The foot* 9, 3 (1999), 115-119.

[6] Plank, M. The pattern of forefoot pressure distribution in hallux valgus. *The foot* 5, 1 (1995) 8-14.

[7] Hurn, S.E., Vicenzino, B., Smith, M.D., Functional impairments characterizing mild, moderate, and severe hallux valgus. *Arthrit Care Res* 67, 1 (2015), 80-88.

[8] Koller, U., Willegger, M., Windhager, R., Wanivenhaus, A., Trnka, H.J., and Schuh, R. Plantar pressure characteristics in hallux valgus feet. *J Orthop Res* 32, 12 (2014), 1688-1693.

[9] Platzer, W., and Kahle, W. *Color Atlas and Textbook of Human Anatomy: Locomotor system, Color Atlas and Textbook of Human Anatomy.* New York, 2002.

[10] Wu, L. Nonlinear finite element analysis for musculoskeletal biomechanics of medial and lateral plantar longitudinal arch of Virtual Chinese Human after plantar ligamentous structure failures. *Clin Biomech* 22, 2 (2007), 221-229.

[11] Cheung, J.T.M., Zhang, M., Leung, A.K.L., and Fan, Y.B. Three-dimensional finite element analysis of the foot during standing—a material sensitivity study. *J Biomech* 38, 5 (2005), 1045-1054.

[12] Perry, J., and Burnfield, J.M. Gait analysis: normal and pathological function. Slack, New Jersey, 1993.

[13] Arnold, E.M., Ward, S.R., Lieber, R.L., and Delp, S.L. A model of the lower limb for analysis of human movement. *Ann Biomed Eng* 38, 2 (2010), 269–79.

[14] Yu, J., Cheung, J.T.M., Fan, Y., Zhang, Y., Leung, A.K.L., and Zhang, M. Development of a finite element model of female foot for high-heeled shoe design. *Clin Biomech* 23, (2008), S31-S38.

[15] Keyak, J.H., and Rossi, S.A. Prediction of femoral fracture load using finite element models: an examination of stress-and strain-based failure theories. *J Biomech* 33, 2 (2000), 209-214.

[16] Glasoe, W.M., Nuckley, D.J., and Ludewig, P.M. Hallux valgus and the first metatarsal arch segment: a theoretical biomechanical perspective. *Phys Ther* 90, 1 (2010), 110.

[17] Zhang, M., and Fan, Y.B. *Computational Biomechanics of the Musculoskeletal System*. CRC Press, 2014.

[18] Piqué-Vidal, C., Solé, M.T., and Antich, J. Hallux valgus inheritance: pedigree research in 350 patients with bunion deformity. *J Foot Ankle Surg* 46, 3 (2007), 149-154.

[19] Perera, A., Mason, L., and Stephens, M. The pathogenesis of hallux valgus. *J Bone Joint Surg Am* 93, 17 (2011), 1650-1661.

Yan Zhang, M.Sc. (Ph.D. student): Lodz University of Technology, Department of Automation, Biomechanics and Mechatronics, Stefanowskiego 1/15, 90-924 Lodz, Poland (*zhangyannbu@gmail.com*).

Jan Awrejcewicz, Professor: Lodz University of Technology, Department of Automation, Biomechanics and Mechatronics, Stefanowskiego 1/15, 90-924 Lodz, Poland (*jan.awrejcewicz@p.lodz.pl*).